Contactless Energy Transmission for an Isolated 100W Gate Driver Supply of a Medium Voltage Converter

R. Steiner*, P. K. Steimer*, F. Krismer** and J.W. Kolar**
*ABB Switzerland Ltd.
Power Electronics and MV Drives, Turgi, Switzerland
**Swiss Federal Institute of Technology – ETH
Power Electronics Systems Laboratory, Zürich, Switzerland
Email: reto.steiner@ch.abb.com

***Abstract*— In this paper, an innovative DC-DC converter is investigated which provides electrical power to the gate driver units of medium voltage level converters. For the discussed DC-DC converter, a galvanic isolation (isolation voltages of up to 35 kV) is required. This electrical isolation is achieved with a coreless transformer in order to obtain a cost-effective solution. Furthermore, the DC-DC converter contains a full-bridge converter being operated with low switching losses, a resonant compensation network to achieve a high overall efficiency and an output side rectifier. In this paper, the design of the coreless transformer, the appropriate compensation networks and the power electronics are discussed in detail. Moreover, measurement results obtained from a 100 W prototype, operated at a switching frequency of 410 kHz, are presented. With the proposed setup, a high overall efficiency of up to 80% and a transformer breakdown voltage of 55 kVrms is achieved. Thus, the proposed converter concept represents a very competitive solution with respect to the typically employed DC-DC converters with dry-type cast coil transformers.**

***Index Terms*—GUSP gate unit power supply, insulation coordination, contactless energy transmission, coreless power transformer**

I. Introduction

With the rising system voltages of medium voltage power converters, the effort to realize gate driver supplies increases significantly in order to withstand high isolation voltages. For a given three-phase medium voltage inverter topology, a maximum isolation voltage of 35 kV is specified for the gate driver supply units and thus galvanic isolation is required for these supply units.

Strict safety requirements must be maintained with respect to the galvanic isolation, since very high voltages occur on the low voltage bus in case of a breakdown of the galvanic isolation. These presumably damage the connected low voltage devices and may even endanger human life. The required safety regulations are given in [1].

The galvanic isolation is typically achieved with dry-type cast coil transformers. The quality of the cast has to be very good, because small air leaks, like cavities and delaminations, could lead to partial discharge and damage the insulation in foreseeable time. For that reason, an isolated and resonant DC-DC converter with a coreless transformer – a so-called inductive coupled power transfer (ICPT) system – is proposed, instead. A large air gap between primary and secondary transformer winding is employed in order to achieve the required dielectric strength. The DC-DC converter is supplied from a low voltage bus (LV bus: 48 VDC) – the same bus that is already used to supply the existing control devices (Fig. 1).

ICPT systems are generally loosely coupled. To reach the needed power density, it is necessary to operate at high frequency. Moreover, reactive power compensation on the primary and the secondary side of the ICPT is needed to attain improved power transfer characteristics.

This paper describes a new method to supply energy to gate units (GU) of medium voltage converters. In order to achieve a high efficiency of the coreless transformer, the coordination of the required insulation and the criteria to minimize the needed isolation distance are discussed in Section II. In Section III, an appropriate DC-DC converter topology is proposed and the converter design is detailed.

Due to the simple and low-cost transformer construction, the investigated isolated power supply is advantageously employed for the supply of gate units of medium voltage converters (5 kV – 35 kV), in general.

II. Fundamental Analysis

A. Insulation Coordination

For security reasons, the galvanic isolation has to withstand three voltage tests. How these tests have to be performed can be found in the standards of the international electrical commission [1].

The impulse voltage test simulates switching and lightning impulses and is characterized by the peak voltage, the rise time and the decay time to half value. In [1], the rise time of the test impulse voltages is 1.2 µs and the decay time to half value 50 µs, which is mostly written like (1.2/50 µs). The peak values of the impulse voltages according to overvoltage category III and reinforced insulation can be found in Table I.

The a.c. voltage test simulates overvoltages. The isolating

Preprint of IECON 2009 Proceedings

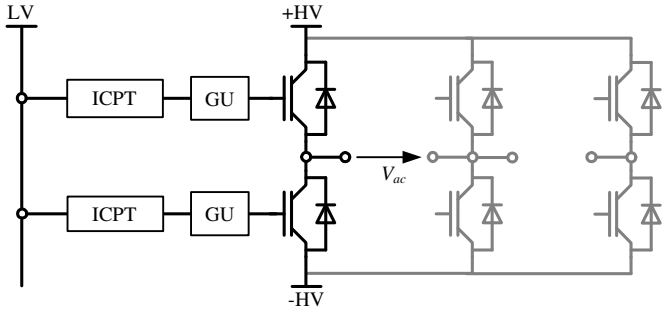

Fig. 1. Application Example

distance has to withstand the given a.c. voltage for a certain time period, with the only condition, that there is no breakdown.

The partial discharge test assures no partial discharge in the solid insulation during working state and has to be done "if the recurring peak working voltage across the insulation is greater than 750 V and the voltage stress on the insulation is greater than 1 kV/mm" (see p. 41 in [1]).

B. Dielectric Breakdown in Air Between Bar Conductors

The critical field strength in dry air and at atmospheric pressure is about 2.5 kV/mm. With exceeding this value, ionization enters which leads to avalanche discharging. The ionization is described with the impact ionization coefficient α and the recombination coefficient η. If the number of free electrons in the heads of the avalanches between two bare conductors exceeds the value N_{crit}, which are about 10^6 to 10^8 free electrons, there is a possibility of breakdown. This behavior is described in the streamer criteria (1), where x_{crit} is the distance between the conductors [2].

$$\int_0^{x_{crit}} (\alpha - \eta)\,dx \geq ln(N_{krit}) \tag{1}$$

TABLE I
TEST AND IMPULSE VOLTAGES

system voltage [kVrms]	a.c. test voltage [kVrms]	impulse voltage [kVpeak]	needed air gap [mm]
6	16	53	5
14	36.4	108	10
20	54	130	20
35	91	200	50

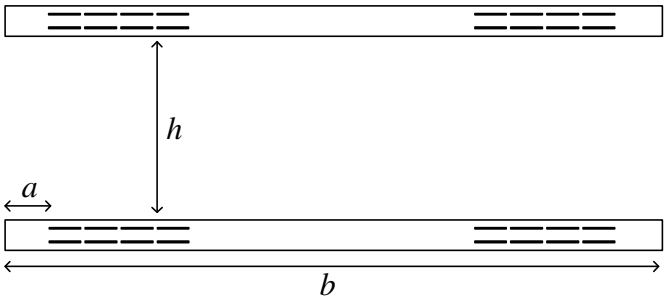

Fig. 2. Construction of the air transformer

C. Solid Insulated Conductors

By isolating the conductors with solid insulation, the dielectric voltage strength can be raised. The solid insulation for printed circuits boards (PCB) is often FR-4, which has a dielectric strength about 20 kV/mm [3]. In the worst case, the air gap is short-circuited by an electric spark and consequently the solid conductor insulation must withstand the total applied voltage. Therefore, appropriate conductor insulation material has to be selected in order to avoid electrical breakdown in case of the impulse and test voltages being applied. These voltages simulate temporary fault conditions and cause partial discharges in the solid insulation. If the solid insulation withstands the voltage test and the impulse test, then the air gap can be minimized, provided that surface discharge is avoided with the working voltage being applied. Continuing surface discharge would stress the solid insulation and accelerate the aging.

The minimal needed air gap for different system voltages is presented in Table I. These values are obtained with an electrostatic finite element simulation using the setup shown in Fig. 2 with a primary and a secondary side transformer winding (h is the air gap, b = 70 mm and a = 5 mm). The thickness of FR-4 on the conductors is 1 mm. The air gap increases at a progressive rate compared to the system voltage because of boundary effects.

The galvanic isolation of the proposed transformer setup (Fig. 2) consists of three different insulation parts. These are the primary and the secondary side winding insulations (FR-4) and the isolation due to the air gap h. The three respective capacitance values can be approximately calculated with the equation used for the plate capacitor:

$$C = \varepsilon_r \varepsilon_0 \frac{A}{d} \tag{2}$$

(ε_r is the relative permittivity, A the plate area and d the thickness of the insulation). Since the air gap h is several times larger than the thickness of the solid insulation and since the relative permittivity of air is smaller than that of FR-4, its capacitance is much smaller than the insulation capacitance. Thus, in the case of non-ionized air, the isolation voltage between primary and secondary windings is virtually only applied to the air gap. Consequently, a comparably small voltage is applied to the solid insulation under operating conditions, so the partial discharge test [1] can be omitted.

We would like to emphasize that an adequate air gap between the windings is needed in order to avoid partial discharge in the solid insulation. The solid insulation part supports the dielectric voltage strength of all overvoltage conditions and also homogenizes the electric field in air, which in turn allows a reduced air gap length h.

D. Structure and Characteristic Quantities of the Coreless Transformer

The coils of the coreless transformer are placed on a multilayer PCB with the windings being located in the middle layers (Fig. 2). The conductors are completely surrounded by

solid insulation which leads to the desired insulation section: solid insulation – air – solid insulation.

The PCB layout, the dimensions of the coils, the track width and the copper thickness have to be selected with respect to the maximum allowable power losses. Therefore, a sufficiently large coupling coefficient between primary and secondary side windings and minimal high frequency conduction losses are required. With a larger coupling coefficient, the primary side apparent power consumption decreases. Consequently the primary side RMS current becomes smaller, which reduces the dissipated power. The coupling coefficient increases with the surface of the coils and decreases with the air gap length h, but does not significantly vary with the track width and height [3]. Varying the track width and height has a strong influence on the coil resistance. The d.c. resistance is proportional to the cross-section conductor area and the length of the track. Because of the high employed switching frequency (cf. Table II), the impact of skin and proximity effects must be considered in order to accurately determine the high frequency conduction losses. For commercially available multilayer PCBs, the copper thickness of the tracks is mostly limited to 210µm. Based on this track thickness, the optimal track width has to be calculated. Increasing the track width leads to a decreased d.c. resistance, however, the high frequency a.c. resistance increases. Conversely, a smaller track width results in a larger d.c. resistance while the high frequency a.c. effects decrease.

Many other shapes and layouts are possible to construct the windings, but the practicability needs to be studied.

The self inductances L_p, L_s and the mutual inductance M of the transformer can be calculated with [5]

- Flux Method
- Neumann's Formula
- Finite elements approach

Integration of the magnetic inductance B over the winding area A results in the flux ϕ through the coil. With the known current $i(t)$, which generates the calculated flux, and the number of turns, the inductance L can be calculated.

$$\phi = \int B \mathrm{d}A \;\Rightarrow\; L = \frac{N\phi}{i(t)} \tag{3}$$

The advantage of the flux method is its descriptive nature when calculating the inductance L. However, for the regarded coreless transformer, different parts of the total flux ϕ are linked to different parts of the transformer coils. Thus, the calculation of L using (3) becomes considerably difficult.

The Neumann's formula (4) is more suitable for a coreless transformer construction. It expresses the mutual inductance between two wires with the length l_1 and l_2 (Fig. 3), where μ_0 is the permeability of vacuum.

$$M_{21} = \frac{\mu_0}{4\pi} \oint\oint \frac{\overrightarrow{\mathrm{d}l_1} \cdot \overrightarrow{\mathrm{d}l_2}}{|\vec{r}_2 - \vec{r}_1|} \tag{4}$$

With the use of the self-inductances of the conductors and the inductance matrix, the primary self-inductance L_p, the secondary self-inductance L_s and the mutual inductance M can be calculated [6].

The transferable power of the transformer for a resistive load and a given primary current can be calculated with

$$P = \frac{1}{2} U_{s,oc} I_{s,sc} = \frac{1}{2} \omega \frac{M^2}{L_s} {I_p}^2 = \frac{1}{2} k^2 \omega L_p {I_p}^2, \tag{5}$$

where $U_{s,oc}$ is the open circuit voltage and $I_{s,sc}$ the short circuit voltage for a given primary current I_p. According to (5), the transferable power P is proportional to the square of the coupling coefficient and proportional to the frequency ω. P increases with increasing L_p and thus enhanced transformer volume is required for a larger P.

The demanded apparent power in air is

$$S_{Air} = \omega M I_p I_s \tag{6}$$

which is determined using the equivalent transformer circuit depicted in Fig. 4. Without the use of a resonant compensation network connected to the high frequency transformer, S_{Air} is several times bigger than the maximal transferable power. The amount of reactive power can be considerably reduced with a reactive power compensation network.

E. Reactive Power Compensation

The aim of the reactive power compensation is to enhance the power transfer capability and voltage source characteristic at the output. In [7] it is found that the SP compensation topology (S denotes a serial compensation capacitor at the primary side, and P denotes a parallel compensation at the secondary side) allows for a constant output voltage which is fully independent on the load resistance R_L. The drawback of the SP compensation topology is, however, that a DC inductor is required at the converter output, which debases the system dynamics.

With the SS compensation topology (the second S denotes a serial compensation capacitor at the secondary side), no output DC inductor is required and still a very stiff output voltage can be achieved. There are two disadvantages related to this compensation technology: the source still needs to supply reactive power and the constant primary current always produces constant losses in the primary coil which reduces the efficiency at part load. Finally, the SS compensation topology

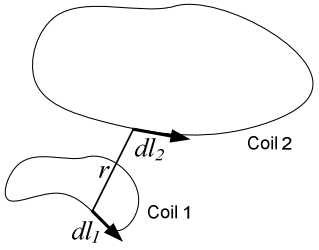

Fig. 3. Two arbitrary coils

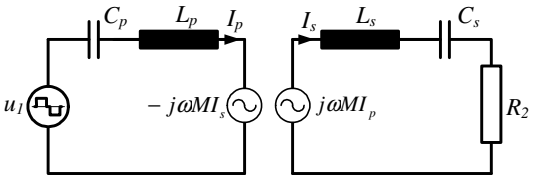

Fig. 4. Coupling model

has been chosen since the advantages considerably prevail the disadvantages. There, the secondary side rectifier – which can be replaced with an equivalent resistance – does not effect the secondary side resonance frequency. Besides, multiple pick ups are easily realizable with the SS compensation topology [8].

With perfect reactive power compensation on the secondary side, the output power is

$$P = \omega M I_p I_s \tag{7}$$

and thus equal to S_{Air}. Equation (7) as well describes the rated power of the coreless transformer by inserting the maximal primary and secondary currents.

In Fig. 4 and Fig. 5, I_s is approximated using a sinusoidal current waveform due to the low-pass properties of the L_s-C_s filter. Thus the well-known approximation for the diode rectifier,

$$\hat{u}_{2,(1)} = \frac{4}{\pi} U_{out}, R_2 \approx \frac{8}{\pi^2} R_L \tag{8}$$

can be used (U_{out} is the output voltage of the rectifier, R_L the load resistance and R_2 the resulting equivalent resistance).

III. General Design Consideration

A. Operational Frequency

High operational frequency is needed to achieve the required output power and a compact design. Therefore a topology has to be chosen which enables the power switches to operate with small switching losses. To minimize the needed switching power, it is important to use power switches with a small total gate charge Q_G and a low effective drain to source capacitance C_{DS}.

The chosen topology is a full bridge converter and the employed control strategy is the so-called zero voltage transition method (*ZVT*)[9]. With ZVT, a high frequency three-level voltage can be generated whereas the resulting transformer current frequency is equal to the switching frequency. In particular, very low switching losses are achieved. Thus, the ZVT method enables switching frequencies up to the MHz range.

B. Concept

The design method is based on [8]. Within here, the design procedure is outlined for the employed converter prototype. The schematic of the prototype is shown in Fig. 5.

The idea is, to select C_s such that the secondary side resonant frequency is equal to the operational frequency. Therefore, the secondary side induced voltage $j\omega MI_p$ is directly applied to R_2, which represents the rectifier and the load (8). In this case, the secondary side impedance (secondary side transformer winding inductance + compensation capacitance C_s + load) is purely resistive and thus solely active power is transmitted over the air.

A primary resonant frequency

$$\omega_p = \frac{1}{\sqrt{L_p C_p}} < \omega \tag{9}$$

lower than the operational frequency is chosen. On these conditions, the network impedance observed at the output of the primary side full bridge contains an inductive part, so ZVT can be achieved. If the inductive part is sufficient large, then the RMS value of I_p varies only slightly in dependence of the applied load [8], which is considered advantageous with respect to the operation with ZVT.

C. Design Method

In the first step, the needed apparent power S_p is calculated (10) to obtain the primary current.

$$S_p = \sqrt{P_p{}^2 + Var_p{}^2} \approx \sqrt{(P_2)^2 + (Q_p P_2)^2} = U_1 I_p \tag{10}$$

Q_p describes the ratio between Var_p and P_2, $Q_p = Var_p / P_2$; in the design example Q_p = 1.2. A larger Q_p increases the stiffness of the output voltage, but as well increases the required reactive power.

The input voltage U_1 is chosen to 48 V, so with a maximum duty cycle of D = 0.94

$$U_1 = \frac{4}{\pi} \frac{U_{in}}{\sqrt{2}} D = 40\text{V}. \tag{11}$$

With (10), the needed primary current I_p is 3.7 A.

In a second step, a primary coil, which is able to conduct I_p, has to be selected. With the resulting coil and the reactive power

$$Var_p = I_p^2 \left(\omega L_p - \frac{1}{\omega C_p} \right), \tag{12}$$

the required capacitance of the primary compensation capacitor can be calculated.

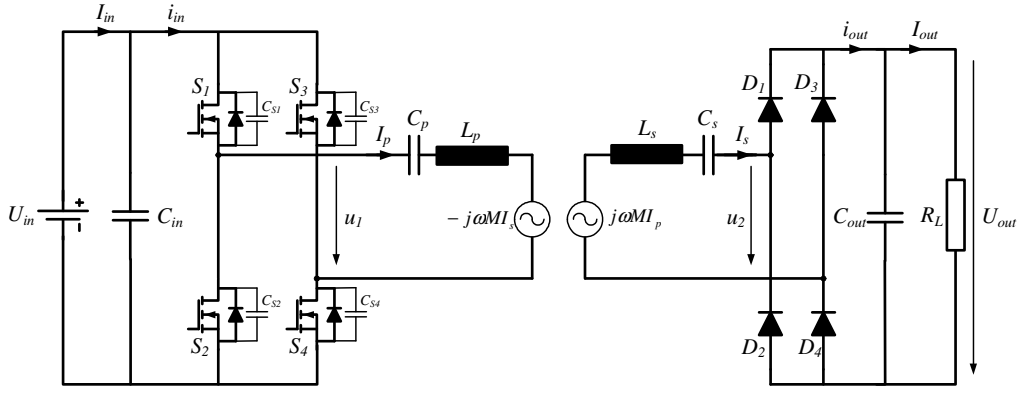

Fig. 5. Schematic of the proposed DC-DC converter

(a)

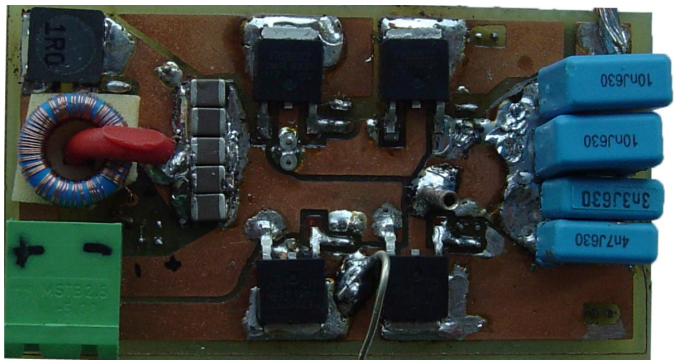

(b)

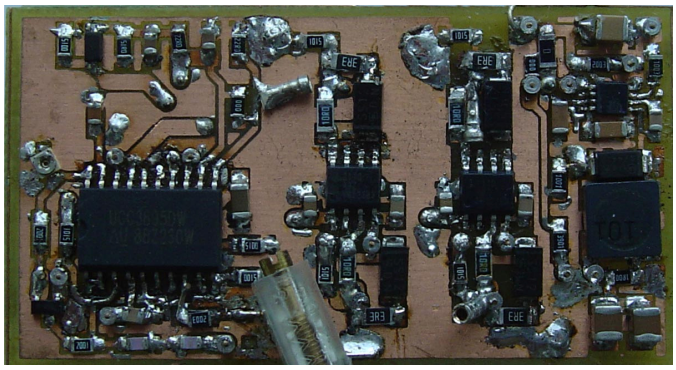

(c)

Fig. 6. (a) Coreless transformer, (b) ZVT full bridge, power part and (c) control board

$$C_p = \frac{1}{\omega^2 L_p - \omega \dfrac{Var_p}{I_p^2}} = 27\text{nF} \tag{13}$$

With U_{out} = 30V and (8) U_2 = 27V results, which is equal to the voltage induced on the secondary side since the secondary side resonant frequency ω_s is tuned to the operational frequency.

$$U_2 = \omega M I_p \tag{14}$$

Therefore, M is equal to

$$M = \frac{U_2}{\omega I_p} = \frac{27\text{V}}{2\pi 400\text{kHz} \cdot 3.7\text{A}} \approx 2.5\mu\text{H} \tag{15}$$

which is obtained by adapting the secondary side coil. If this coil is not realizable, L_p has to be adapted.

IV. Experimental Results

A. Voltage Test

A partial discharge test and an a.c.-voltage test have been performed to verify the dielectric voltage strength. Test voltages of up to 60 kV_{rms} were provided by a high voltage transformer within a shielded room and the connecting cables have been fed through power line filters.

TABLE II
Parameters of the Prototype

Nominal frequency	410kHz
Rated Power	100W
Primary rated current	2.7A_{rms}
Secondary rated current	3.9A_{rms}
Rated load	6.5Ω
d.c. coil resistance	150mΩ
a.c. coil resistance (410kHz)	450mΩ
Primary inductance	9.38µH
Primary capacitance	28nF
Mutual inductance	2.51µH
Secondary inductance	9.88µH
Secondary capacitance	19.9nF

Even though, the final transformer PCBs will consist of multilayer PCBs with a copper thickness of 210µm, double-sided PCBs with a copper thickness of 105µm have been used for the first prototype of the coreless transformer in order to allow for an economically reasonable verification of the presented design (Fig. 6 (a)). The thickness of the employed FR-4 is 1.6 mm. The air gap can be varied between 20 mm and 50 mm. In order for the prototype transformer to pass the voltage test, an additional FR-4 isolation coating has been applied to both sides of the PCB.

Partial discharge tests have been performed for the setup with different air gaps. Surface discharge has been noted whenever the electrical field close to the PCB exceeded the critical electrical field strength of air. This result coincides with the results obtained from simulations.

For an air gap of 20 mm, the a.c. voltage has been raised up to the breakdown voltage, which was measured to be equal to 55 kV_{rms}. The breakdown voltage is high enough to ensure the standards [1] for a system voltage of 20 kV_{rms}, and agrees to the calculations. During breakdown, the resulting arc even occurred across the connections, so a properly isolated cabling is of uttermost importance.

B. Efficiency and Output Voltage

The efficiency and the output voltage have been measured with the setup shown in Fig. 6. The full-bridge converter, operated with ZVT, is realized using two double-sided PCBs (30 mm x 60 mm, Fig. 6 (b) and (c)). With a four-layer PCB, the presented full-bridge converter could readily be implemented on a single board, since each PCB is only populated on a single side. Very low conduction and switching losses occur in the employed MOSFETs and therefore no additional heatsinks are required except for the copper surfaces close to the power switches shown in Fig. 6 (b).

The air transformer is constructed according to Fig. 2 and Fig. 6 (a) with an air gap of 20mm. The same primary and secondary side coils are employed, with a PCB size of 60 mm x 160 mm and 8 turns; rectangular type windings with a thickness of 105µm and a width of 3.25mm are used. Even though, this first prototype of the coreless transformer (Fig. 6

(a)) is constructed with a double-sided PCB, it is suitable to verify the proposed energy transmission. However, without additional isolation, it would not pass the voltage test, since the tracks have to be completely surrounded by FR-4.

The rectifier is realized on a 30 mm x 60 mm double-layer PCB. The measured and rated parameters of the prototype are summarized in Table II.

In Fig. 7 (a) the output voltage u_1 of the full-bridge and the primary current i_p are plotted under full load conditions. The total converter efficiency and the output voltage are plotted in dependence on the output power in Fig. 7 (b). The output voltage remains within an acceptable range between 25 V to 31 V except for the case of no load operation. There, the self resonance of the secondary side inductance leads to an increased output voltage.

The efficiency is close to 80% between part load and full load operation and drops considerably for small load conditions, due to a large amount of circulating power on the primary side. The biggest losses occur in the coils. For an output power of 100W the loss distribution is approximately: 2.5W in the full-bridge, 20W in the coreless transformer and 4W in the rectifier.

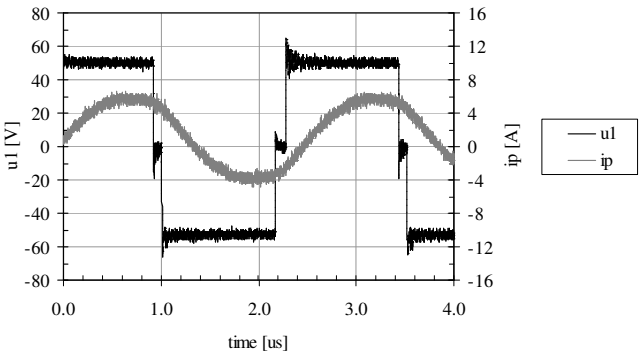

(a)

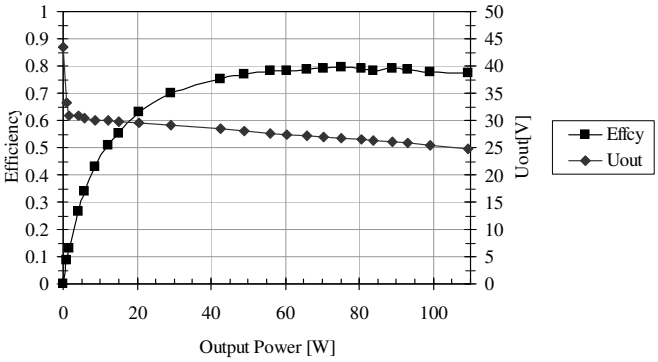

(b)

Fig. 7. (a) Efficiency and output voltage, (b) u_1 and i_p by full-load operation

V. Conclusion

With a simple and cost-effective DC-DC converter, a gate unit power supply can be realized which permanently withstands isolation voltages of up to 35 kV. The proposed converter topology allows for a low-cost replacement of the expensive cast coil transformer with the presented coreless transformer, which is considered an enormous advantage for medium voltage converters. With the use of high switching frequencies, a compact design is achieved, whereas high efficiency is still feasible due to the employed ZVT control scheme. It has been shown, that the transformer copper losses account for the biggest part of the total losses and therefore future design refinements mainly need to consider improvements with respect to the geometry of the employed transformer windings.

References

[1] IEC, "Adjustable speed electrical power drive systems – Part 5-1: Safety requirements – Electrical, thermal and energy", Reference number IEC 61800-5-1:2007

[2] Beyer, W. Boeck, K. Möller, W. Zaengl, "Hochspannungstechnik: Theoretische und praktische Grundlagen für die Anwendung", Springer Verlag Berlin, 1986

[3] S. Malrieu, P. Notingher jr, F. Pacreau, A. Toureille "Influence of Space Charge on the Breakdown of Mulilayered Epoxy: A Study by the Thermal Step Method", *IEEE Annual Report – Con. On Elect. Insulation and Dielectric Phenomena,* October 1997

[4] S. C. Tang, S. Y. Hui, Henry Shu-Hung Chung, "Characterization of Coreless Printed Circuit Board (PCB) Transformers", *IEEE Trans. Power Electron.*, vol. 15, no. 6, pp. 1275-1282, Nov. 2000

[5] M. Jufer, N. Macabrey, M. Perrottet, "Modeling and test of contactless inductive energy transmission", Mathematics and Computation in Simulation 46, pp. 197-211, 1998

[6] N. Hemche, A. Jaafari, "Wireless Transmission of Power Using a PCB Transformer with Mobile Secondary", *IEEE Mediterranean Electr. Conf.*, pp. 629-634, 2008

[7] Chwei-Sen Wang, Oskar H. Stielau, and Grant A. Covic, "Design Considerations for a Contactless Electric Vehicle Battery Charger", *IEEE Trans. Power Electron.,* vol. 52, no. 5, pp. 1308-1314, Oct. 2005

[8] Xun Liu and S. Y. (Ron) Hui, "Optimal Design of a Hybrid Winding Structure for Planar Contactless Battery Charging Platform", *IEEE Trans. Power Electron.,* vol. 23, no. 1, pp. 455-463, Jan. 2008

[9] Bill Andreycak, "Phase Shifted, Zero Voltage Transition Design Considerations and the UC3875 PWM Controller", Application Notes, May 1997